Designing cyclic competence-stimulating peptide (CSP) analogs with pan-group quorum-sensing inhibition activity in *Streptococcus pneumoniae*

Yifang Yang[a], Jingjun Lin[b], Anthony Harrington[a], Gabriel Cornilescu[c], Gee W. Lau[b,1], and Yftah Tal-Gan[a,1]

[a]Department of Chemistry, University of Nevada, Reno, Reno, NV 89557; [b]Department of Pathobiology, University of Illinois at Urbana–Champaign, Urbana, IL 61802; and [c]National Magnetic Resonance Facility at Madison, University of Wisconsin–Madison, Madison, WI 53706

Edited by Richard P. Novick, New York University School of Medicine, New York, NY, and approved December 12, 2019 (received for review September 13, 2019)

Streptococcus pneumoniae **is an opportunistic human pathogen that utilizes the competence regulon, a quorum-sensing circuitry, to acquire antibiotic resistance genes and initiate its attack on the human host. Interception of the competence regulon can therefore be utilized to study *S. pneumoniae* cell–cell communication and behavioral changes, as well as attenuate *S. pneumoniae* infectivity. Herein we report the design and synthesis of cyclic dominant negative competence-stimulating peptide (dnCSP) analogs capable of intercepting the competence regulon in both *S. pneumoniae* specificity groups with activities at the low nanomolar range. Structural analysis of lead analogs provided important insights as to the molecular mechanism that drives CSP receptor binding and revealed that the pan-group cyclic CSPs exhibit a chimeric hydrophobic patch conformation that resembles the hydrophobic patches required for both ComD1 and ComD2 binding. Moreover, the lead cyclic dnCSP, CSP1-E1A-cyc(Dap6E10), was found to possess superior pharmacological properties, including improved resistance to enzymatic degradation, while remaining nontoxic. Lastly, CSP1-E1A-cyc(Dap6E10) was capable of attenuating mouse mortality during acute pneumonia caused by both group 1 and group 2 *S. pneumoniae* strains. This cyclic pan-group dnCSP is therefore a promising drug lead scaffold against *S. pneumoniae* infections that could be administered individually or utilized in combination therapy to augment the effects of current antimicrobial agents.**

quorum sensing | *Streptococcus pneumoniae* | competence-stimulating peptide | cyclic peptides

Streptococcus pneumoniae (pneumococcus) is an important human pathogen that causes a range of severe diseases such as bacteremia, meningitis, and pneumonia (1–3). *S. pneumoniae* mainly affects humans with immature or compromised immune systems, including young children, the elderly, and patients with immunodeficiency disorders (4, 5). A myriad of antibiotics and, more recently, pneumococcal conjugate vaccines were introduced to fight pneumococcal infections. However, these therapies generated a strong selection pressure that promoted the development of antibiotic-resistant and vaccine-escape pneumococci (6–10). A major contributor to the development of antibiotic resistant and vaccine-escape strains is the ability of *S. pneumoniae* to enter the competent state, where the competent pneumococcal cells can lyse noncompetent bacteria, take up DNA from the environment, and incorporate it into its genome (11–15). This genetic plasticity is critical for *S. pneumoniae* to cope with environmental stress and allows rapid evolution of resistant strains.

The competence state in *S. pneumoniae* is regulated by the competence regulon, a quorum-sensing (QS) circuit mediated by the competence-stimulating peptide (CSP) (16). The precursor peptide of CSP encoded by the *comC* gene is cleaved and exported out of the cell by the ABC transporter ComAB (17). CSP accumulates extracellularly as the population increases, and, when the concentration of CSP reaches a threshold, it can effectively bind and activate a transmembrane histidine kinase receptor ComD (18–20). There are multiple variants of CSP and ComD, but the majority of pneumococcal strains utilize either CSP1 or CSP2, with their compatible receptors ComD1 and ComD2, respectively, resulting in two specificity groups among *S. pneumoniae* (21, 22). Each CSP has high selectivity toward its compatible receptor, leading to very limited cross-talk between these two specificity groups (23–25). On activation, ComD autophosphorylates and activates its cognate response regulator ComE through phosphorylation (26). Phosphorylated ComE initiates the transcription of numerous genes, including the alternative sigma factor *comX*, which is responsible for the induction of competence for genetic transformation (27–31). Although competence for genetic transformation is the most widely studied cellular process regulated by the competence regulon, recent studies indicated that this QS circuit also controls virulence and biofilm formation, suggesting that this circuitry can be targeted to attenuate pneumococcal infection (32–34).

Initially discovered in *Vibrio fischeri*, QS is a ubiquitous mechanism that allows bacteria to assess their population density and alter gene expression once they reach high cell number (35–38). In Gram-positive bacteria, QS circuitries generally rely on peptide-based

Significance

Streptococcus pneumoniae **is a prevalent human pathogen that is a major cause of community-acquired pneumonia. *S. pneumoniae* utilizes the competence regulon to initiate its attack on the human host. In the current manuscript, we report 1) the design of cyclic competence-stimulating peptide analogs capable of inhibiting the competence regulon in *S. pneumoniae* with activities at the low nanomolar range; 2) structural analysis that elucidated the molecular mechanism of lead analogs; and 3) pharmacological evaluation of a lead analog that revealed that the peptide can attenuate *S. pneumoniae*-mediated acute pneumonia in vivo. Our results highlight the potential of inhibiting the competence regulon as a therapeutic approach to combat pneumococcus infections.**

Author contributions: G.W.L. and Y.T. designed research; Y.Y., J.L., A.H., and G.C. performed research; Y.Y., J.L., A.H., and G.C. analyzed data; and Y.Y., G.W.L., and Y.T. wrote the paper.

The authors declare no competing interest.

This article is a PNAS Direct Submission.

Published under the PNAS license.

Data deposition: Atomic coordinate files, assigned chemical shift files, experimental restraints used for structure determination and refinement, and NOESY peak lists have been deposited in the BioMagResBank, www.bmrb.wisc.edu (accession nos.: CSP1-cyc(K6D10), 30593; CSP1-cyc(Orn6D10), 30594; CSP1-cyc(Dab6E10), 30595; CSP1-cyc(Dap6E10), 30601; and CSP1-E1A-cyc(Dap6E10), 30690).

[1]To whom correspondence may be addressed. Email: geelau@illinois.edu or ytalgan@unr.edu.

This article contains supporting information online at https://www.pnas.org/lookup/suppl/doi:10.1073/pnas.1915812117/-/DCSupplemental.

First published January 8, 2020.

Downloaded at Palestinian Territory, occupied on December 22, 2021

www.manaraa.com

signaling molecules to initiate the QS response. The involvement of QS in bacterial pathogenesis in many prevalent human pathogens has led to significant efforts to intercept QS circuitries as a potential antivirulence therapeutic approach (35, 39–41). The accessory gene regulator (agr) QS circuitry in *Staphylococcus aureus* was one of the first Gram-positive systems to be targeted. Seminal work by Novick, Muir, and coworkers revealed the role of the agr QS circuitry in *S. aureus* pathogenesis (42, 43). This work has laid the foundation for the development of autoinducing peptide-based agr QS inhibitors and their utilization by the same research group, as well as others, to attenuate virulence phenotypes (44–47). The fsr QS circuit in *Enterococcus faecalis* is another system that was explored for its therapeutic potential. Work by Murray and coworkers linked the fsr circuitry with biofilm formation and virulence factor production (48, 49), and has sparked efforts to utilize the native signal, gelatinase biosynthesis-activating pheromone, as a scaffold for the development of QS modulators capable of lessening pathogenic phenotypes (50–53). Lastly, the competence regulon was found to be a rather ubiquitous circuitry in streptococci, controlling the acquirement of genetic material from the environment, biofilm formation, bacteriocin production, and, in pathogenic streptococci, virulence factor production (39, 54, 55). Indeed, significant efforts were made by us and others to characterize the competence regulon in different streptococci species and utilize the corresponding CSP signals to develop QS modulators with therapeutic potential (56–59).

The therapeutic potential of targeting the competence regulon in pneumococcus was demonstrated by both Lau and Tal-Gan groups in two separate studies (60, 61). In these studies, we found that CSP1-E1A, a dominant-negative analog of CSP1 (dnCSP) identified by Lau and coworkers, and CSP2-E1Ad10, a CSP2 analog identified by Tal-Gan and coworkers, can strongly inhibit the ComD1 and ComD2 receptors, respectively, in a cell-based reporter gene assay. Moreover, CSP1-E1A and CSP2-E1Ad10 attenuated the production of virulence factors in vitro, and reduced mouse mortality during acute pneumonia by ComD1 (group 1) and ComD2 (group 2) pneumococcal strains, respectively. These results suggest that synthetic CSP-based dnCSPs capable of disrupting the CSP:ComD interaction can be used to control pneumococcal infections. However, both CSP1-E1A and CSP2-E1Ad10 exhibited significantly reduced cross-group inhibition activity as well as low stability toward enzymatic degradation, limiting their therapeutic potential. Therefore, to effectivity attenuate pneumococcal infectivity in vivo, a pan-group QS inhibitor with enhanced stability against proteolytic degradation is required. Herein, we report the design of a potent pan-group pneumococcal QS inhibitor, CSP1-E1A-cyc(Dap6E10), through peptide cyclization. CSP1-E1A-cyc(Dap6E10) also displays significantly improved proteolytic stability and the ability to strongly attenuate virulence factor expression and mouse mortality during acute pneumonia in both group 1 and group 2 pneumococcal strains.

Results and Discussion

Designing a Pan-group Activator. Our previous structural studies of CSP1 and CSP2 revealed that an α-helix structure is critical to the ability of CSPs to induce QS response. Specifically, the α-helix structure is important to the formation of two distinct hydrophobic patches that are critical to ComD1 and ComD2 binding (62). Based on the structural studies, we hypothesized that the specific conformation of each side chain within the hydrophobic patches has a significant effect on the binding affinity to each receptor, and proposed that the hydrophobic patches formed by CSP1 and CSP2-d10, the most potent ComD1 and ComD2 activators, respectively, are optimal for ComD1 and ComD2 binding. Therefore, starting with the side-chain residues that form the hydrophobic patch of CSP1, conformational modification and fine-tuning could lead to the stabilization of a hydrophobic patch that is optimal for both ComD1 and ComD2 binding, resulting in a pan-group QS activator. Then, by replacing the Glu1 residue, whose side chain was shown to be critical for receptor activation, with alanine, we can convert this pan-group activator to a pan-group inhibitor (25).

Our strategy of modifying the conformation of the hydrophobic patch in CSP1 was to utilize peptide cyclization through side-chain residues in certain positions in CSP1 to stabilize the α-helix structure. We hypothesized that systematic macrocycle ring size alteration would then allow us to gradually modify the conformation of the α-helix structure, thus fine-tuning the conformation of the hydrophobic patch and the activity of the peptide. To this end, we first set out to determine the most suitable position for peptide cyclization. Our structure–activity relationship (SAR) analysis revealed several positions that are both dispensable and situated about a multiple of 3.6 residues from one another (the length of one α-helix turn), and thus can be utilized for peptide cyclization. We therefore conducted a ring position scan where we incorporated orthogonally protected lysine and aspartic acid in different positions (6 and 9, 6 and 10, 10 and 14, and 6 and 14) and coupled them together to form lactam macrocycles (Fig. 1*B*). Biological evaluation of the four cyclic peptides, along with their precyclic counterparts, revealed that all of the modifications to the CSP1 sequence were detrimental, leading to significant reduction in activity (Table 1 and *SI Appendix*, Table S8). Of the four cyclic peptides, CSP1-cyc(K6D10), which differs from CSP1 only in having K6 and D10 coupled through their side chains to afford the macrocycle, exhibited the most promising biological activity against ComD1 and ComD2. We therefore selected this scaffold for further optimization.

Next, we set out to optimize the conformation of CSP1-cyc(K6D10) by systematically altering the ring size and bridge position of the macrocycle region. We therefore replaced K6 with ornithine (Orn), 2,4-diaminobutyric (Dab), and 2,3-diaminopropionic acid (Dap), while replacing D10 with Glu to afford a library of seven analogs bearing macrocycles with ring sizes varying from 17 to 21 atoms (Fig. 1*B*). Biological evaluation of the cyclic library, along with the precyclic counterparts, revealed that a ring size of 18 to 19 atoms is optimal for activating the ComD1 receptor (Table 1). Interestingly, replacement of Lys at position 6 with Dap resulted in a potent, linear pan-group activator (*SI Appendix*, Table S8), suggesting that the shorter side chain is beneficial for ComD2 binding. However, constraining this analog through cyclization resulted in almost complete abolishment of activity, suggesting that a macrocycle of 17 atoms is too short to accommodate the required bioactive conformation (Table 1). Indeed, structural evaluation of both peptides using circular dichroism revealed a significant drop in helicity for the cyclic peptide compared with its precyclic counterpart (*SI Appendix*, Fig. S12). Moreover, it was clear that the bridge position is critical for activating ComD2, as all of the analogs bearing Asp at position 10 were relatively inactive against the ComD2 receptor, while the analogs bearing Glu at position 10 and having ring sizes of 18 to 19 atoms were highly active against the ComD2 receptor (Table 1). Most importantly, we found two potent pan-group activators, CSP1-cyc(Dap6E10) and CSP1-cyc(Dab6E10), with activities comparable to CSP1 and CSP2 in activating the ComD1 and ComD2 receptors, respectively.

Structural Analysis of Select Cyclic Peptide Analogs. As mentioned above, we hypothesized that inducing and stabilizing a hydrophobic patch that resembles those of both CSP1 and CSP2-d10 would lead to pan-group QS modulators. We therefore set out to test whether our newly discovered cyclic pan activators, CSP1-cyc(Dap6E10) and CSP1-cyc(Dab6E10), possess hydrophobic patches that resemble those of CSP1 and CSP2-d10. To this end, we selected four cyclic peptide analogs, two relatively inactive analogs, CSP1-cyc(K6D10) and CSP1-cyc(Orn6D10),

Downloaded at Palestinian Territory, occupied on December 22, 2021

www.manaraa.com

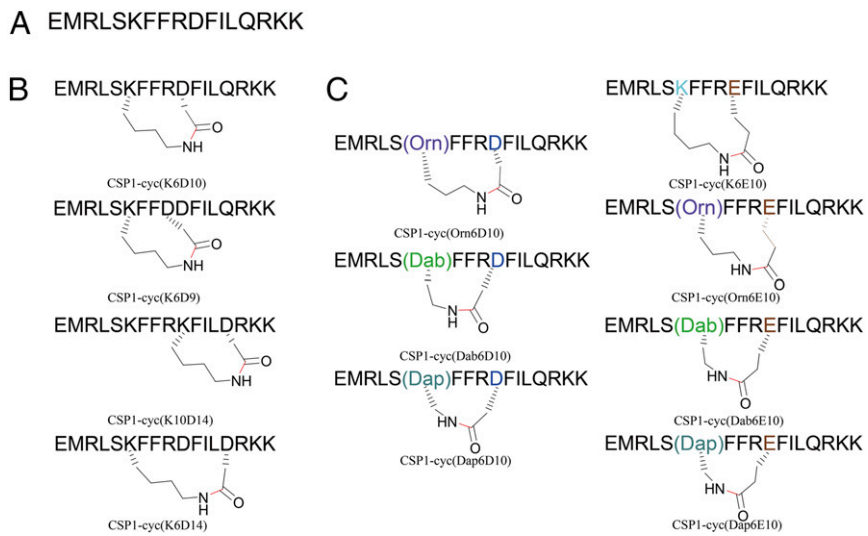

Fig. 1. (*A*) Amino acid sequence of CSP1. (*B*) Simplified structures of the ring-position scan cyclic CSP1 analogs. (*C*) Simplified structures of the ring-size and bridge position scan cyclic CSP1 analogs.

and the two most potent analogs, CSP1-cyc(Dap6E10) and CSP1-cyc(Dab6E10), and determined their three-dimensional (3D) solution structures using 2D NMR spectroscopy. We then overlaid and compared the hydrophobic patches formed by each cyclic peptide analog with those of CSP1 and CSP2-d10.

First, we compared the hydrophobic patches formed by the cyclic peptides with the proposed hydrophobic patch for effective ComD1 binding. CSP1-cyc(K6D10) is a weak ComD1 activator, which has an EC_{50} value of 258 nM and 44% of maximal induction of *comX* compared to CSP1. Therefore, we expected that CSP1-cyc(K6D10) would exhibit a significantly different hydrophobic patch compared to the one CSP1 displays. Indeed, the hydrophobic patch of CSP1-cyc(K6D10) (63) aligns poorly with that of CSP1, with only the L4 and F11 residues aligning relatively well (Fig. 2*A*; RMSD of 3.44 Å for residues 4, 7, 8, 11 and 12). CSP1-cyc(Orn6D10), which has an EC_{50} value of 193 nM and 100% of maximal induction of *comX* compared to CSP1, exhibited improved activity compared to CSP1-cyc(K6D10). Consistent with the trend, the hydrophobic patch of CSP1-cyc(Orn6D10) (64) aligned better with the CSP1 patch, except the I12 residue (Fig. 2*B*; rmsd of 3.74 Å for residues 4, 7, 8, 11, and 12). Lastly, CSP1-cyc(Dab6E10) (65) and CSP1-cyc(Dap6E10) (66), both of which exhibited activities comparable to CSP1, possess hydrophobic patches that align well with the CSP1 patch for all five residues (Fig. 2 *C* and *D*; rmsd of 2.37 and 1.92 Å for residues 4, 7, 8, 11, and 12).

Next, we compared the hydrophobic patches of the cyclic peptides with the proposed hydrophobic patch for effective ComD2 binding. CSP1-cyc(K6D10) and CSP1-cyc(Orn6D10) are only weak activators of the ComD2 receptor. We therefore expected that their hydrophobic patches comprising F7, F8, F11, I12 and L13 would align poorly with the hydrophobic patch of CSP2-d10, the most potent ComD2 activator identified to date. Indeed, only the F8, F11, and L13 residues in CSP1-cyc(K6D10) align, although poorly, with L9, F11, and L13 in the CSP2-d10 hydrophobic patch (Fig. 3*A*), while only F11 and L13 in CSP1-cyc(Orn6D10)

Table 1. EC_{50} values of cyclic CSP1 analogs against the ComD1 and ComD2 receptors

		EC_{50} (nM)* (95% CI)†	
Name	Ring size (atoms)	ComD1	ComD2
CSP1		10.3 (6.27 to 16.8)	526 (498 to 556)
CSP2		1,650 (1,190 to 2,300)	50.7 (40.6 to 63.2)
CSP1-cyc(K6D9)	17	>1000	528 (211 to 1318)
CSP1-cyc(K10D14)	20	257 (196 to 340)	–‡
CSP1-cyc(K6D14)	32	>1000	>1,000
CSP1-cyc(K6D10)	20	258 (203 to 328)	>1,000
CSP1-cyc(Orn6D10)	19	193 (136 to 275)	>1,000
CSP1-cyc(Dab6D10)	18	59.5 (38.1 to 93.2)	>1,000
CSP1-cyc(Dap6D10)	17	435 (237 to 796)	>1,000
CSP1-cyc(K6E10)	21	350 (259 to 474)	>1,000
CSP1-cyc(Orn6E10)	20	422 (386 to 461)	>1,000
CSP1-cyc(Dab6E10)	19	12.2 (11.1 to 13.6)	31.4 (29.3 to 33.7)
CSP1-cyc(Dap6E10)	18	14.6 (9.27 to 23.1)	13.1 (6.79 to 25.1)

See *Materials and Methods, Biological Reagents and Strain Information* and *Materials and Methods, beta-Galactosidase Assays* for detail of reporter strains and methods. See *SI Appendix* for plots of agonism or antagonism dose–response curves. All assays were performed in triplicate.

*EC_{50} values determined by testing peptides over a range of concentrations.

†The 95% confidence interval.

‡EC_{50} not determined due to the analog's low activity (*SI Appendix*, Figure S8).

Downloaded at Palestinian Territory, occupied on December 22, 2021

www.manaraa.com

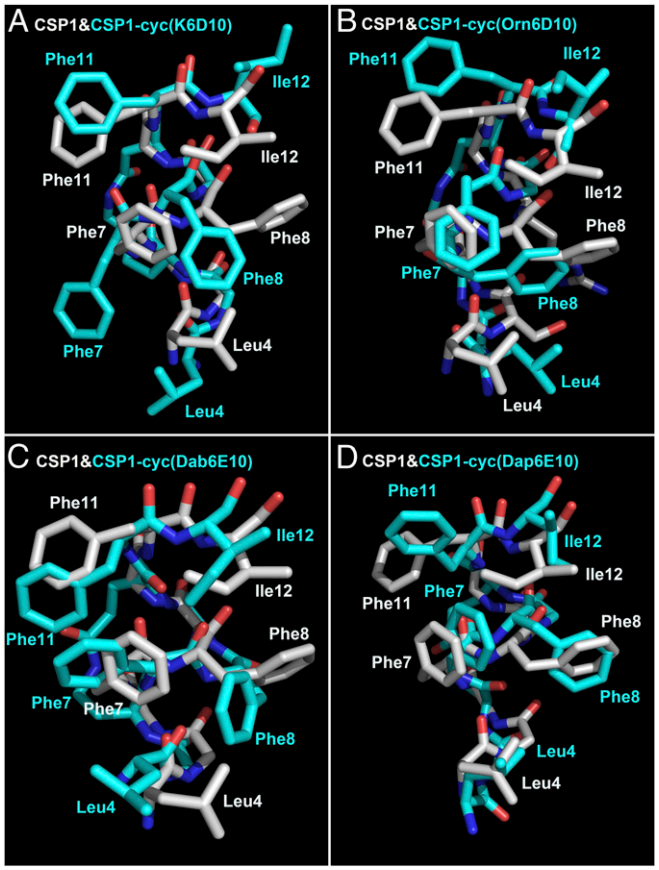

Fig. 2. (*A*) Overlay of CSP1 (silver) and CSP1-cyc(K6D10) (cyan; BMRB accession ID 30593) structures. (*B*) Overlay of CSP1 (silver) and CSP1-cyc(Orn6D10) (cyan; BMRB accession ID 30594) structures. (*C*) Overlay of CSP1 (silver) and CSP1-cyc(Dab6E10) (cyan; BMRB accession ID 30595) structures. (*D*) Overlay of CSP1 (silver) and CSP1-cyc(Dap6E10) (cyan; BMRB accession ID 30601) structures. Residues E1-R3 and L13-K17, as well as the side chains of S5 and R9 in the cyclic peptide structures, and the side chains of S5, K6, R9, and D10 in CSP1, are hidden for clarity.

align, although poorly, with F11 and F13 in the CSP2-d10 hydrophobic patch (Fig. 3*B*). In contrast, because CSP1-cyc(Dab6E10) and CSP1-cyc(Dap6E10) are very potent ComD2 activators, we expected that their hydrophobic patches would align well with the hydrophobic patch that CSP2-d10 exhibits. Indeed, we found that the F7, F8, F11, I12, and L13 residues in both cyclic peptides overlay well with the I8, L9, F11, L12, and F13 residues in CSP2-d10, respectively (Fig. 3 *C* and *D*). Together, our structural analysis reaffirmed the validity of our previously hypothesized hydrophobic patches that are required for effective ComD1 and ComD2 binding, as well as confirming that the conformation of the hydrophobic patch can be fine-tuned by changing the macrocycle ring size, thus fine-tuning the activity of the peptides.

Converting Pan-group Activators into Pan-group Inhibitors. The main goal in this study was to develop pan-group QS inhibitors. Therefore, we utilized the two lead pan-group activators, CSP1-cyc(Dab6E10) and CSP1-cyc(Dap6E10), as scaffolds for the construction of QS inhibitors. As previously described, replacement of Glu1 with Ala was found to convert CSPs to competitive inhibitors. We therefore replaced Glu1 in CSP1-cyc(Dab6E10) and CSP1-cyc(Dap6E10) with alanine to produce CSP1-E1A-cyc(Dab6E10) and CSP1-E1A-cyc(Dap6E10). Biological evaluation revealed that CSP1-E1A-cyc(Dab6E10) can only effectively inhibit the ComD1 receptor (Table 2). Significantly, to our satisfaction, CSP1-E1A-cyc(Dap6E10) was found to inhibit the ComD1 receptor with potency comparable to the most potent ComD1 inhibitor, CSP1-E1A, and the ComD2 receptor with an IC_{50} value only threefold higher than the most potent ComD2 inhibitor, CSP2-E1Ad10, making it a potent pan-group inhibitor of pneumococcal QS (Table 2) (25). Structural analysis of CSP1-E1A-cyc(Dap6E10) (67) using 2D NMR spectroscopy revealed that, although the side-chain residues forming the hydrophobic patch appear to be more clustered together than in the corresponding activator, CSP1-cyc(Dap6E10) (Fig. 4 *C* and *D*; rmsd of 2.93 Å between CSP1-E1A-cyc(Dap6E10)) and CSP1-cyc(Dap6E10) for residues 4, 7, 8, 11, and 12), the inhibitory peptide still presents a hydrophobic patch that resembles the patches required for both ComD1 (Fig. 4*A*; rmsd of 2.77 Å for residues 4, 7, 8, 11, and 12) and ComD2 binding (Fig. 4*B*).

CSP1-E1A-cyc(Dap6E10) Exhibits Significantly Enhanced Proteolytic Stability. To evaluate the potential utility of CSP1-E1A-cyc(Dap6E10) as a therapeutic agent, we tested its proteolytic stability to degradation by trypsin/chymotrypsin. CSP1 and the precyclic precursor, CSP1-E1AK6DapD10E, were also tested in the same conditions for comparison. All three peptides exhibited similar half-lives, suggesting that the cyclization does not improve the stability of the peptide (Fig. 5). However, analysis of the degradation products of the three peptides revealed that this is not the case. Following 4 h of incubation, analysis of CSP1 degradation revealed products corresponding to the breaking of the amide bonds between residues 3 and 4, 6 and 7, 9 and 10, and 15 and 16. Similarly, after

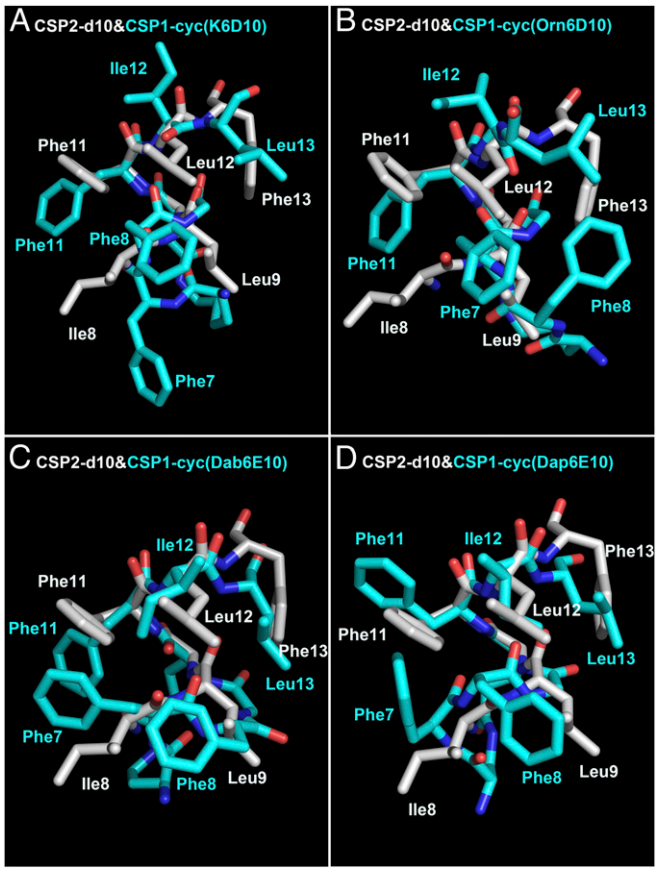

Fig. 3. (*A*) Overlay of CSP2-d10 (silver) and CSP1-cyc(K6D10) (cyan) structures. (*B*) Overlay of CSP2-d10 (silver) and CSP1-cyc(Orn6D10) (cyan) structures. (*C*) Overlay of CSP2-d10 (silver) and CSP1-cyc(Dab6E10) (cyan) structures. (*D*) Overlay of CSP2-d10 (silver) and CSP1-cyc(Dap6E10) (cyan) structures. Residues E1-S5 and Q14-K17 of the cyclic peptide, residues E1-I7 and L14-K17 of CSP2-d10, the side chain of R9 in the cyclic peptide structures, and the side chain of D10 in the CSP2-d10 structures are hidden for clarity.

Downloaded at Palestinian Territory, occupied on December 22, 2021
www.manaraa.com

Table 2. IC_{50} values of cyclic CSP1 analogs against the ComD1 and ComD2 receptors

Name	Ring size (atoms)	IC_{50} (nM)*,† (95% CI†) ComD1	ComD2
CSP1-E1A-cyc(Dab6E10)	19	173 (136 to 221)	>1,000
CSP1-E1A-cyc(Dap6E10)	18	75.8 (49.9 to 115)	182 (132 to 251)
CSP1-E1A-des-K16K17-cyc(Dap6E10)	18	7.57 (3.60 to 15.9)	67.2 (42.0 to 107)

See *Materials and Methods, Biological Reagents and Strain Information* and *Materials and Methods, beta-Galactosidase Assays* for detail of reporter strains and methods. See *SI Appendix* for plots of agonism or antagonism dose–response curves. All assays performed in triplicate.
*IC_{50} values determined by testing peptides over a range of concentrations.
†The 95% confidence interval.

4 h of incubation, analysis of the degradation products of CSP1-E1AK6DapD10E revealed that the same amide bonds were cleaved. In contrast, in the case of CSP1-E1A-cyc(Dap6E10), breakage of the amide bonds was only observed between residues 3 and 4, as well as 15 and 16, suggesting that peptide cyclization confers resistance to enzymatic degradation of the macrocycle region (*SI Appendix*, Figs S9–S11). Additionally, mass spectrometry (MS) analysis indicated that, after 4 h, the majority of CSP1-E1A-cyc(Dap6E10) undergoes hydrolysis between residues 15 and 16, leading to the formation of CSP1-E1A-des-K16K17-cyc(Dap6E10). We have previously shown that the K16 and K17 residues are dispensable and do not affect the activity of the native CSPs (25), suggesting that CSP1-E1A-des-K16K17-cyc(Dap6E10) may still be a potent pan-group inhibitor. To test this, we synthesized the degradation product, CSP1-E1A-des-K16K17-cyc(Dap6E10), and evaluated its biological activity. Surprisingly, the truncated analog exhibited almost 10-fold higher inhibition potency against the ComD1 receptor and threefold higher inhibition potency against the ComD2 receptor compared to the parent CSP1-E1A-cyc(Dap6E10) (Table 2). Together, our results suggest that the "effective half-life" of CSP1-E1A-cyc(Dap6E10), the half-life of the parent peptide and its active degradation product, is significantly longer than 4 h. Unfortunately, due to the poor water solubility of CSP1-E1A-des-K16K17-cyc(Dap6E10), we were not able to measure its half-life and therefore the exact "effective half-life" of CSP1-E1A-cyc(Dap6E10).

Modulation of Pneumolysin Release by CSP1-E1A-cyc(Dap6E10). Previously, we have shown that activation of the competence regulon leads to expression of competent state-specific allolytic factors, including LytA, CbpD, and CibAB that release an important pneumococcal virulence factor, pneumolysin (68), which plays an important role during an acute pneumonia model of infection. Additionally, CSP1-E1A and CSP2-E1Ad10 competitively inhibit the release of pneumolysin and pneumolysin-induced hemolysis in the group 1 strain D39 and group 2 strain TIGR4, respectively (60, 61); however, both peptides exhibit significantly reduced cross-group inhibition activity. We therefore examined the efficacy of CSP1-E1A-cyc(Dap6E10) to cross-inhibit pneumolysin-mediated hemolysis of sheep blood (Hemostat Laboratories #DSB250) induced by CSP1 in the group 1 strain D39 and by CSP2 in the group 2 strain TIGR4. As expected, the pneumolysin-deficient mutant Δ*ply*, as well as ComX-deficient mutant Δ*comX1*Δ*comX2* and the allolysis-deficient mutant Δ*lytA*Δ*cbpD*Δ*cibAB*, did not express pneumolysin and did not cause measurable levels of hemolysis (Fig. 6). In contrast, provision of CSP1 to D39 and CSP2 to TIGR induced significant levels of hemolysis. Significantly, CSP1-E1A-cyc(Dap6E10) attenuated pneumolysin release and effectively reduced the hemolysis of sheep blood in both D39 and TIGR4 exposed to CSP1 and CSP2, respectively (Fig. 6), demonstrating its pan-inhibitory capability. CSP1-E1A-cyc(Dap6E10) was threefold to fourfold more effective in inhibiting hemolysis mediated by D39 than TIGR4, in agreement with its IC_{50} values against both strains. Collectively, these results suggest that CSP1-E1A-cyc(Dap6E10) could be efficacious in attenuating pneumococcus virulence during host infection.

CSP1-E1A-cyc(Dap6E10) Attenuates Acute Lung Infection by Both Groups 1 and 2 Pneumococci. Before determining the efficacy of CSP1-E1A-cyc(Dap6E10) in attenuating pneumococcal infections, we first examined the toxicity of the peptide. CD1 mice (five per cohort) were intratracheally inoculated with CSP1-E1A-cyc(Dap6E10) (50 μg/d) for 1 wk. Systemic toxicity was assessed by performing blood chemistry and complete blood count (CBC) with differential at the University of Illinois College of Veterinary Medicine Clinical Pathology Laboratory. Major organs (lungs, hearts, livers, kidneys, and spleens) and sternum (genotoxicity) were analyzed histopathologically as we have previously published (69). Importantly, toxicity studies revealed no myelosuppression, renal injury, hepatic toxicity, or other abnormalities (Fig. 7 *A*–*D*; data not shown) in mice exposed to all native and modified CSPs, supporting previous findings by us and others that they are nontoxic (60, 61, 70). Next, we examined the ability of CSP1-E1A-cyc(Dap6E10) to attenuate acute pneumonia infection by D39 and TIGR4. Previously, we have shown that CSP1-E1A and CSP2-E1Ad10 could protect against mortality during acute pneumonia caused by D39 and TIGR4, respectively (60, 61). CD1 mice (cohorts of 15 to 20 mice) were intranasally infected with D39 or TIGR4 (5×10^6 colony-forming units [CFU] per mouse). Two hours after infection, D39-infected mice were treated with 50 μL of sterile saline (0.9% NaCl), CSP1-E1A-cyc(Dap6E10), or CSP2-E1Ad10, whereas TIGR4-infected mice were treated with saline, CSP1-E1A-cyc(Dap6E10), or CSP1-E1A (100 μg per mouse, in 50 μL doses), and their survival was monitored. Infected mice treated with saline or incompatible dnCSPs exhibited a near-100% mortality rate within 144 h postinfection (Fig. 7 *E* and *F*), revealing the limitation of group-specific dnCSPs in protecting against infection by pneumococcus expressing differing CSP and ComD variants. Importantly, mice infected with D39 and TIGR4 and treated with CSP1-E1A-cyc(Dap6E10) exhibited significantly higher survival and delayed kinetics in mortality (Fig. 7 *E* and *F*), highlighting the therapeutic potential of pan-dnCSPs in attenuating pneumococcal infections.

Conclusions

To summarize, *S. pneumoniae*, a notorious human pathogen that rapidly evolves to evade current treatment strategies, including vaccination and antimicrobial agents, utilizes the competence regulon QS circuitry to initiate pneumolysin release during acute pneumonia to erode the air–blood barrier and penetrate the blood stream, resulting in bacteremic pneumonia. Inhibition of the competence regulon can therefore be used to attenuate pneumococcal infections without inducing strong selective pressure for resistance development. Herein, we utilized rational design in combination with conformational optimization strategies to develop pan-group CSP-based QS modulators with activities in the low nanomolar range. Our lead dnCSP, CSP1-E1A-cyc(Dap6E10), was found to be a superior drug lead compound, exhibiting improved resistance to enzymatic degradation while remaining

Downloaded at Palestinian Territory, occupied on December 22, 2021

www.manaraa.com

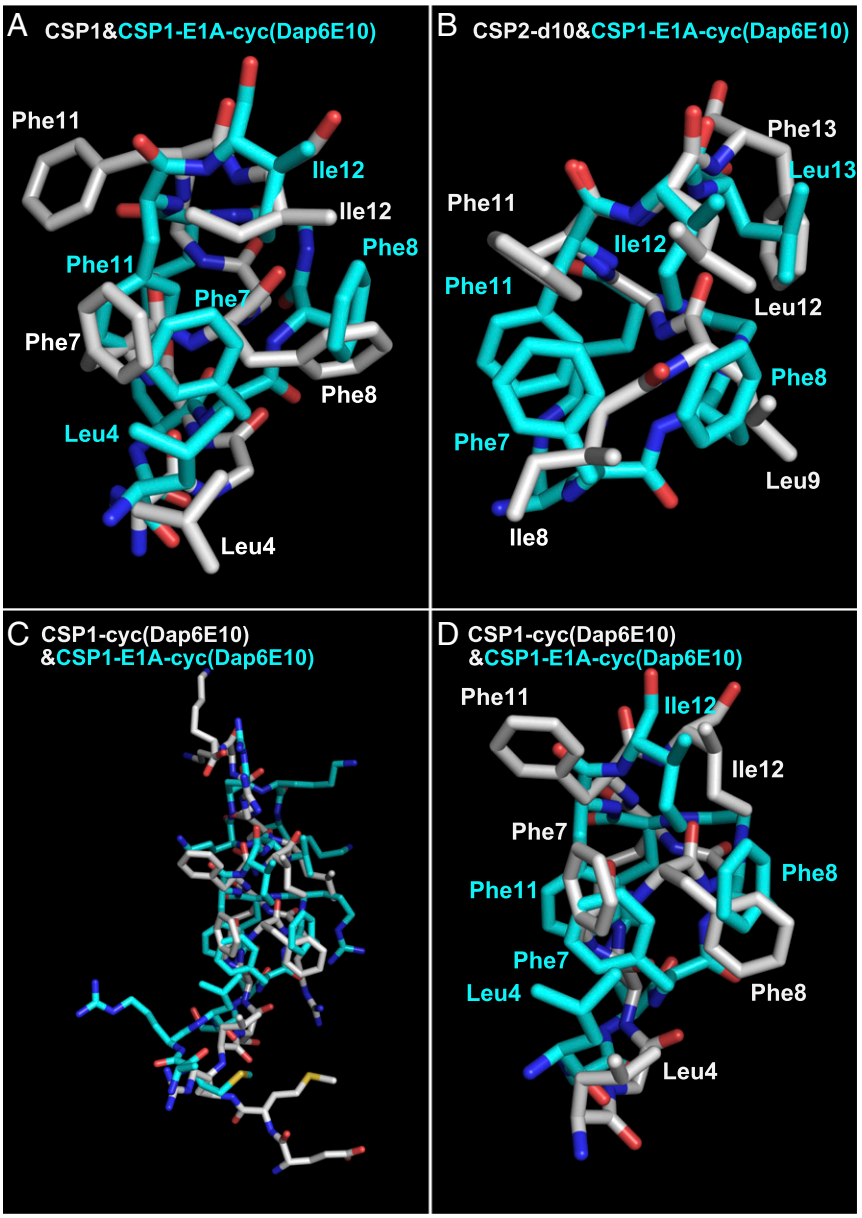

Fig. 4. (*A*) Overlay of CSP1 (silver) and CSP1-E1A-cyc(Dap6E10) (cyan; BMRB accession ID 30690) structures. (*B*) Overlay of CSP2-d10 (silver) and CSP1-E1A-cyc(Dap6E10) (cyan) structures. (*C*) Overlay of CSP1-cyc(Dap6E10) (silver) and CSP1-E1A-cyc(Dap6E10) (cyan) structures. (*D*) Overlay of CSP1-cyc(Dap6E10) (silver) and CSP1-E1A-cyc(Dap6E10) (cyan) structures emphasizing the hydrophobic patch regions. In *A*, *B*, and *D*, residues E1-R3 and L13-K17 (E1-S5 and Q14-K17 in *B*) of the cyclic peptide, residues E1-R3 and L13-K17 of CSP1, residues E1-I7 and L14-K17 of CSP2-d10, the side chain of R9 (S5 and R9 in *A* and *D*) in the cyclic peptide structures, the side chains of S5, K6, R9, and D10 in the CSP1 structure, and the side chain of D10 in the CSP2-d10 structure are hidden for clarity.

nontoxic. Importantly, this highly potent pan-group dnCSP was capable of attenuating mouse mortality during acute pneumonia caused by both group 1 and group 2 pneumococcus. With the rapid increase in antibiotic resistance development, coupled with the fact that current pneumococcal antimicrobial agents were found to activate the competence regulon in sublethal concentrations, a paradigm shift in pneumococcus treatment strategies is needed. CSP1-E1A-cyc(Dap6E10) is therefore uniquely situated to combat pneumococcus infections, either as the sole agent or in combination with current antimicrobial agents. Successful implementation of CSP1-E1A-cyc(Dap6E10) as a therapeutic agent could pave the way to the development of additional QS-based antiinfective therapeutics against a variety of human pathogens, desperately needed in the stagnant antimicrobial landscape.

Materials and Methods

Data Availability Statement. With the exception of the NMR structural coordinates, which are publicly available at the Biological Magnetic Resonance Data Bank (BMRB) structural databank, all data and protocols reported are contained in the manuscript and *SI Appendix*.

Chemical Reagents and Instrumentation. All chemical reagents and solvents were used as previously described (25). Briefly, chemical reagents and solvents were purchased from Sigma-Aldrich and used without further purification, water (18 MΩ) was purified using a Millipore Analyzer Feed System, and solid-phase resins were purchased from Advanced ChemTech and Chem-Impex International.

Reversed-phase high-performance liquid chromatography (RP-HPLC) and MS were performed as previously described (25). Briefly, RP-HPLC was performed using a Shimadzu system equipped with a CBM-20A communications bus module, two LC-20AT pumps, an SIL-20A auto sampler, an SPD-20A

Downloaded at Palestinian Territory, occupied on December 22, 2021
www.manaraa.com

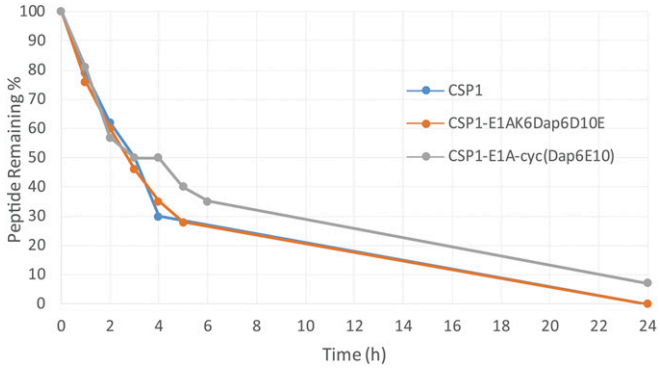

Fig. 5. Metabolic stability of CSP1 analogs. All peptides were treated with trypsin/chymotrypsin (0.05 μg·mL^{-1} enzyme concentration). RP-HPLC was used to monitor peptide degradation. All peptides have a half-life of about 3 h. After 3 to 4 h, precipitation was observed in the solution of CSP1-E1A-cyc(Dap6E10), resulting in the plateau in the curve.

ultraviolet/visible (VIS) detector, a CTO-20A column oven, and an FRC-10A fraction collector. Matrix-assisted laser desorption ionization time-of-flight MS (MALDI-TOF MS) data were obtained on a Bruker Microflex spectrometer equipped with a 60-Hz nitrogen laser and a reflectron. In reflectron positive ion mode, the acceleration voltage on Ion Source 1 was 19.01 kV. Exact mass data were obtained on an Agilent Technologies 6230 TOF LC/MS spectrometer. The samples were sprayed with a capillary voltage of 3,500 V, and the electrospray ionization source parameters were as follows: gas temperature of 325 °C at a drying gas flow rate of 8 L/min at a pressure of 35 psi.

Solid-Phase Peptide Synthesis. Solid-phase peptide synthesis (SPPS) was performed as previously described (25). Briefly, the CSP1 analogs were synthesized using standard Fmoc-based SPPS procedures on 4-benzyloxybenzyl alcohol (Wang) resin. Preloaded Fmoc-L-Lys(Boc) Wang resin (0.343 mmol/g) was used for peptides that required a lysine at the C terminus, and preloaded Fmoc-L-Arg(Pbf) Wang resin (0.305 mmol/g) was used for peptides that required an arginine at the C terminus. Amino acids that have alloc- or allyl-protected amine or carboxyl group on the side chain were added in the selected positions for future cyclization (see *SI Appendix* for the full procedure). Upon completing the construction of the entire peptide sequence, the Fmoc protecting group was kept on the N-terminal amine, while the alloc- and allyl-protected side chains were deprotected with the following protocol. The resin was washed three times with dichloromethane (DCM) for 1 min before it was dried. Then the air in the reaction vessel was replaced with argon. Approximately 5 mL of dry DCM was added to a 15-mL polypropylene centrifuge tube, and the tube was sparged with argon for 3 min. Ten equivalents (equiv.) (relative to the resin loading) of phenyl silane (which is acting as a scavenger) was added to the centrifuge tube, and the tube was sparged with argon for an additional 2 to 3 min. Then 0.5 equiv. of tetrakis(triphenylphosphine)palladium(0) was added to the centrifuge tube, and the tube was sparged with argon for about 4 min. The resulting solution in the centrifuge tube was then added to the resin, and the reaction vessel was covered with aluminum foil and properly sealed. Then, the reaction vessel was placed on a shaker at 200 rpm for 2 h. The vessel was drained, and the resin was washed four times with 0.5% sodium ditethyldithiocarbamate trihydrate in DMF for 2 min with shaking, followed by four washes with DMF for 1 min with shaking. A solution of [ethyl cyano(hydroxyimino)acetato]-tri(1-pyrrolidinyl)-phosphonium hexafluorophosphate (Pyoxim; 1.25 equiv. relative to the resin loading) and *N,N*-Diisopropylethylamine (2.5 equiv. relative to the resin loading) in DMF was then added to the resin to couple the deprotected free amine and carboxyl group to form the macrocycle ring. The reaction vessel was placed on a shaker at 200 rpm for 3 h. The vessel was drained, the solution was replenished, and the reaction was allowed to proceed for 14 h, followed by three washes with DMF. The Fmoc protecting group at the N terminus was removed, and the peptide was cleaved from the resin, along with the side-chain protecting groups (see *SI Appendix* for the full procedure).

Peptide Purification. Crude peptides were purified with RP-HPLC as previously described (25). Briefly, a semipreparative Phenomenex Kinetex C18 column (5 μm, 10 mm × 250 mm, 110 Å) was used for preparative RP-HPLC work, while an analytical Phenomenex Kinetex C18 column (5 μm, 4.6 mm × 250 mm, 110 Å) was used for analytical RP-HPLC work. Standard RP-HPLC conditions were as follows: Flow rates = 5 mL·min^{-1} for semipreparative separations and 1 mL·min^{-1} for analytical separations; mobile phase A = 18 MΩ water + 0.1% trifluoro acetic acid (TFA); mobile phase B = acetonitrile (ACN) + 0.1% TFA. Purities were determined by integration of peaks with UV detection at 220 nm. Preparative HPLC methods were used to separate the crude peptide mixture into different chemical components using a linear gradient (first prep 5% B → 45% B over 40 min, and second prep 20% B → 30% B over 30 min). Then, an analytical HPLC method was used to quantify the purity of the desired product using a linear gradient (5% B → 95% B over 27 min). Only peptide fractions that were purified to homogeneity (>95%) were used for the biological assays. High-resolution MS was used to validate the presence of synthesized peptides. The observed mass-to-charge (*m/z*)

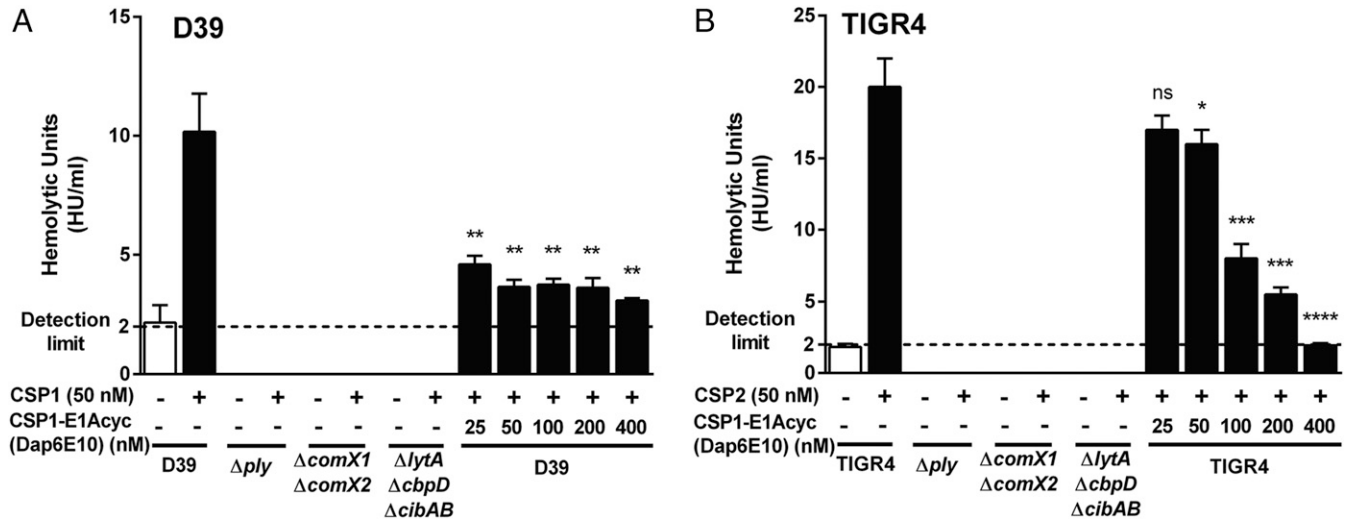

Fig. 6. CSP1-E1A-cyc(Dap6E10) competitively inhibits hemolysis induced by CSPs. (*A*) Group 1 strain D39 and (*B*) group 2 strain TIGR4 and their respective derivatives were treated with 50 nM CSP1 or CSP2 in the presence or absence of increasing concentrations of CSP1-E1A-cyc(Dap6E10). The release of pneumolysin into culture supernatant as manifested by the hemolytic activity was quantified. All experiments were performed in triplicate. Data are shown as the mean ± SEM *$P < 0.05$, **$P < 0.01$, ***$P < 0.001$, or ****$P < 0.0001$ against D39 exposed to CSP1 or TIGR4 exposed to CSP2 as determined by two-way ANOVA with Tukey's multiple comparisons tests. ns, not significant.

Downloaded at Palestinian Territory, occupied on December 22, 2021

www.manaraa.com

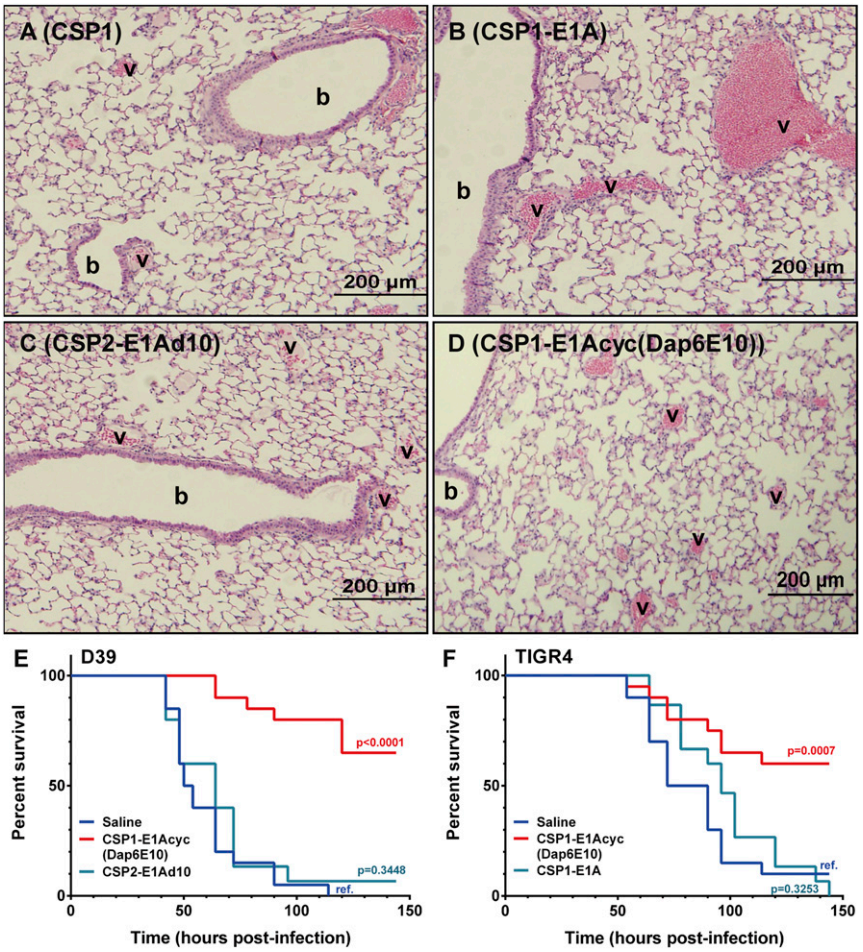

Fig. 7. CSP1-E1A-cyc(Dap6E10) attenuates mouse mortality during acute pneumonia infection. (*A–D*) Both native and dnCSPs did not induce abnormal proinflammatory response in mouse lungs. CD1 mice (cohorts of 5) were intratracheally inoculated with native or each dnCSP (50 μg/d, 1 wk). Lungs were sectioned and stained with H&E; b, bronchioles; v, vessels. (*E* and *F*) CSP1-E1A-cyc(Dap6E10) reduced mouse mortality during acute pneumonia. CD1 mice (cohorts of 15 to 20) were intranasally infected with D39 or TIGR4 (5×10^6 CFU). At 2 h postinfection, mice were treated with sterile saline (0.9% NaCl, $n = 20$), CSP1-E1A (100 μg per mouse, $n = 15$), CSP2-E1Ad10 (100 μg per mouse, $n = 15$), and CSP1-E1A-cyc(Dap6E10) (100 μg per mouse, $n = 20$), and their survival was monitored for 144 h. The indicated *P* values were derived when comparing the mortality of infected mice treated with dnCSPs against those treated with sterile saline by using the Kaplan–Meier Log Rank (Mantel–Cox) survival test. ref, reference.

ratio of the peptide was compared to the expected *m/z* ratio for each peptide (*SI Appendix*, Table S1).

Biological Reagents and Strain Information. All standard biological reagents were used as previously described (25). Briefly, standard biological reagents were purchased from Sigma-Aldrich and used according to enclosed instructions. Donor horse serum (defibrinated) was purchased from Sigma-Aldrich and stored at 4 °C until use in bacterial growth conditions. To examine the ability of the synthesized CSP analogs to modulate the ComD receptors, and thus the competence regulon in *S. pneumoniae*, beta-galactosidase assays were performed using D39pcomX::lacZ (group I) and TIGR4pcomX::lacZ (group II) reporter strains, while phenotypic assays were performed using D39 (group I) and TIGR4 (group II) strains.

Bacterial Growth Conditions. Bacteria were grown as previously described (25). Briefly, frozen stocks were created from 1.5-mL aliquots of pneumococcal bacteria (0.2 optical density [OD] 600_{nm}) in Todd Hewitt Broth (THB) supplemented with 0.5% yeast extract (THY) and 0.5 mL of glycerol, and stored at −80 °C. For experiments, frozen stocks were streaked onto a THY agar plate containing 5% serum and chloramphenicol at a final concentration of 4 μg/mL. The plate was incubated for 8 to 9 h in a CO_2 incubator (37 °C with 5% CO_2). Fresh colonies (single colony for D39pcomX::lacZ; multiple colonies for TIGR4pcomX::lacZ) were transferred to 5 mL of THY broth supplemented with chloramphenicol at a final concentration of 4 μg/mL, and the culture was incubated in a CO_2 incubator overnight (15 h). Overnight cultures were then diluted (1:50 for D39pcomX::lacZ; 1:10 for TIGR4pcomX::lacZ) with THY, and the resulting solution was incubated in a CO_2 incubator for 3 to 4 h, until the bacteria reached exponential stage (0.30 to 0.35 for D39pcomX::lacZ; 0.20 to 0.25 for TIGR4pcomX::lacZ) as determined by using a plate reader.

beta-Galactosidase Assays. All beta-galactosidase assays were performed as previously described (25).

Activation assays. The ability of synthetic CSP1 analogs to activate the expression of *comX* was determined using reporter strains grown in THY (pH 7.3). An initial activation screening was performed at high concentration (10 μM) for all CSP analogs. First, 2 μL of 1 mM solution of CSP analogs in dimethyl sulfoxide (DMSO) were added in triplicate to a clear 96-well microtiter plate. Then, 2 μL of 20 μM solution of CSP1 were added in triplicate and served as the positive control for the group I strain (D39pcomX::lacZ), while 2 μL of 100 μM solution of CSP2 were added as the positive control for the group II strain (TIGR4pcomX::lacZ). These concentrations were chosen to afford full activation of the QS circuit, as determined from the dose-dependent curves created for the native CSPs. Then, 2 μL DMSO were added in triplicate and served as the negative control for both groups. Then, 198 μL of bacterial culture were added to each well containing CSP and analogs, the plate was incubated at 37 °C for 30 min, and the OD 600_{nm} was measured. In order to measure the beta-galactosidase activity in the pneumococcal culture, the cells were lysed by incubating the culture for 30 min at 37 °C with 20 μL of 0.1% Triton X-100. In a new plate, 100 μL of Z-buffer solution (60.2 mM Na_2HPO_4, 45.8 mM NaH_2PO_4, 10 mM

Downloaded at Palestinian Territory, occupied on December 22, 2021
www.manaraa.com

KCl, and 1.0 mM $MgSO_4$ in 18 MΩ H_2O; pH was adjusted to 7.0 and the buffer was sterilized before use) containing 2-nitrophenyl-beta-D-galactopyranoside (ONPG) at a final concentration of 0.4 mg/mL were added, followed by 100 μL of lysate, and the plate was incubated for 3 h at 37 °C. The reaction was stopped by adding 50 μL of 1 M sodium carbonate solution, and the OD 420_{nm} and OD 550_{nm} were measured using a plate reader. The final results were reported as percent activation, which is the ratio between the Miller units of the analog and that of the positive control. For calculation of Miller units, please see data analysis below. The potency of the analogs was evaluated using a dose-dependent assay in which peptide stock solutions were diluted with DMSO in serial dilutions (either 1:2, 1:3, or 1:5) and assayed as described above. GraphPad Prism 5 was used to calculate the EC_{50} values, which are the concentration of a drug that gives half-maximal response.

Inhibition assays. The ability of dnCSPs to inhibit the expression of *comX* by outcompeting CSP for the receptor binding site was evaluated using the same assay conditions as described above, except that the native CSP was added to every well in a set concentration (50 nM CSP1 for group I; 250 nM CSP2 for group II) that was chosen to afford full activation of the QS circuit, as determined from the dose-dependent curves created for the native CSPs. First, 2 μL of native CSP (5 μM solution of CSP1 for group I; 25 μM solution of CSP2 for group II) and 2 μL of 1 mM solution of CSP1 analogs were added to the same well in triplicate in a clear 96-well microtiter plate. Then, 2 μL of native CSP (5 μM solution of CSP1 for group I; 25 μM solution of CSP2 for group II) and 2 μL of DMSO were added to the same well in triplicate and served as the positive control. Then, 4 μL of DMSO were added in triplicate and served as the negative control. Then, 196 μL of bacterial culture were added to the wells, and the plate was incubated at 37 °C for 30 min. The procedure for lysis, incubation with ONPG, and all of the measurements were as described in the activation assay. The inhibition potency of CSP1 analogs was evaluated using a dose-dependent assay where peptide stock solutions were diluted with DMSO in serial dilutions (either 1:2, 1:3, or 1:5) and assayed as described above. GraphPad Prism 5 was used to calculate the IC_{50} values, which are the concentration of an inhibitor where the response (or binding) is reduced by half.

Analysis of activation/inhibition data. Miller units were calculated using the following formula:

$$\text{Miller unit} = 1{,}000 \times \frac{[\text{Abs}_{420} - (1.75 \times \text{Abs}_{550})]}{(t \times v \times \text{Abs}_{600})}.$$

Abs_{420} is the absorbance of *o*-nitrophenol; Abs_{550} is the scatter from cell debris, which, when multiplied by 1.75, approximates the scatter observed at 420 nm; *t* is the duration of incubation with ONPG in minutes; *v* is volume of lysate in milliliters; and Abs_{600} reflects cell density.

NMR Sample Preparation. Peptide samples for structural NMR experiments were prepared as previously described (62). Briefly, the peptides were dissolved in 250 mM deuterated dodecyl phosphocholine (DPC-d_{38}; CDN Isotopes) in a PBS buffer solution with 10% D_2O (Cambridge Isotope Laboratories). The final concentration of the peptides was 1.9 mM. PBS buffer solution was a water solution that contained NaCl (137 mM), KCl (2.7 mM), Na_2HPO_4 (10 mM), and KH_2PO_4 (1.8 mM), and the pH was adjusted to 7.4.

NMR Spectroscopy. All NMR spectra were recorded as previously described (62). Briefly, NMR spectra were recorded on a Bruker 900-MHz spectrometer at 298 K. Spectra were processed using NMR Pipe software. Chemical shifts were referenced to water at 4.771 parts per million (ppm). We acquired the following 2D homonuclear experiments: gradient selection correlation spectroscopy (COSY) with presaturation, total correlation spectroscopy (TOCSY) with decoupling in the presence of scalar interactions (DIPSI) spin-lock, and the 3-9-19 or excitation sculpting with gradient water suppression schemes, ^1H-^{15}N fast heteronuclear single-quantum correlation spectroscopy (HSQC), sensitivity-enhanced ^1H-^{13}C HSQC with selective 180° ^{13}C pulses, nuclear Overhauser effect spectroscopy (NOESY) with flip-back and Watergate water suppression and a 200-ms mixing time, and rotating frame NOESY (ROESY) with continuous wave spin lock and 3-9-19 water suppression and a 200-ms mixing time. The COSY experiments were collected with 1,024 and 2,048 complex and real data points in the direct and indirect dimensions, respectively, with four scans per data point. The TOCSY and ROESY experiments were acquired with 1,024 direct and 512 indirect complex data points, with 80-ms and 200-ms spin lock durations, and with 8 and 16 scans per data point, respectively. The ^1H-^{15}N and ^1H-^{13}C HSQC experiments were collected with 1,024 complex data points and 13-ppm spectral width in the direct dimensions and 128 complex data points with 28-ppm spectral width and 256 complex data points and 150-ppm spectral width in the indirect dimension, with 8 and 16 scans per data point, respectively. A 1-s relaxation delay was used in all experiments except TOCSY (relaxation delay of 1.2 s). Excitation sculpting with gradient water suppression was used in the ^1H 1-D experiment, and 16,000 real data points were acquired, with eight scans per data point.

Spectra Assignment and Structure Calculation. NMR spectra were analyzed as previously described (62). Briefly, all spectra were analyzed with National Magnetic Resonance Facility at Madison (NMRFAM)-SPARKY (71). Assignment of resonances for each peptide was achieved using the standard sequential assignment methodology. The volumes of the NOE peaks were calculated by SPARKY and converted into a continuous distribution of interproton distance restraints, with a uniform 35% distance error applied to take into account spin diffusion (see *SI Appendix*, Table S7 for total number of NOEs divided into backbone vs. side chain for each peptide). The 2D ^1H-^{15}N and ^1H-^{13}C HSQC experiments allowed assigning all backbone (and C^{β}) atoms, which were subsequently used as input in the TALOS-N program to generate backbone dihedral angle restraints (ϕ/ψ) and side-chain chi1 angle restraints (see *SI Appendix* for complete restraint tables used for structural calculations) (72). The 3D structure calculations and refinements made use of the torsion angle molecular dynamics and the internal variable dynamics modules of Xplor-NIH (v. 2.42) (73). Backbone and heavy atom rmsd values were calculated for the 20-structure ensembles of all peptides using the entire peptide sequence (*SI Appendix*, Table S7). PyMOL was used for visual analysis and presentation of the peptide structures.

Stability Assay. To study the enzymatic stability of the CSP1 analogs, the peptides were dissolved in aqueous PBS solution (137 mM NaCl, 2.7 mM KCl, 10 mM Na_2HPO_4, and 1.8 mM KH_2PO_4; pH 7.4) to afford a final concentration of 0.066 mM. Trypsin and chymotrypsin (25 $\mu g \cdot mL^{-1}$) stock solution (diluted from a 2.5 $mg \cdot mL^{-1}$ trypsin solution; Gibco) was made in PBS solution. Protease solution was added to the peptide solution to afford a final concentration of 0.05 $\mu g \cdot mL^{-1}$, and then the solution was incubated with shaking at 37 °C. Aliquots (500 μL) of peptide solution were taken and mixed with ACN/H_2O (1:1, 100 μL) for 0, 1, 2, 3, 4, 5, 6, and 24 h, and then analyzed immediately for peptide degradation by analytical RP-HPLC. During the analytical RP-HPLC runs, the degradation products were manually collected and analyzed by MALDI-TOF MS.

BMRB Accession ID. BMRB accession ID codes are as follows: CSP1-cyc(K6D10), 30593; CSP1-cyc(Orn6D10), 30594; CSP1-cyc(Dab6E10), 30595; CSP1-cyc(Dap6E10), 30601; and CSP1-E1A-cyc(Dap6E10), 30690. Data is available at: http://www.bmrb.wisc.edu and include atomic coordinates, assigned chemical shifts, experimental restraints used for structure determination and refinement, and NOESY peak lists.

Hemolysis Assay. Hemolytic assays were performed as we have published (60, 61, 68). Briefly, pneumococcal strains were cultured in THB to $OD600_{nm}$ of 0.2 and then treated with 50 nM CSP1 or CSP2 with increasing concentration of dnCSPs. Untreated controls were exposed to same volume of sterile PBS. After 20 min of incubation, supernatants were collected by pelleting pneumococcal cells at 3,000 × *g* for 15 min, and cell-free supernatants were filtered through 0.22-μm syringe filters (Millipore). Twofold serial dilutions of the supernatants were performed with fresh THB before incubating with 10 mM dithiothreitol at room temperature for 15 min. Then, a 500-μL aliquot of each sample was mixed with 200 μL of 2% sheep red blood cells and incubated for 30 min at 37 °C. The mixture was centrifuged at 3,000 × *g* for 5 min. The absorbance of the cell-free supernatant was measured at $OD\ 541_{nm}$. The hemolytic units were reported as the highest dilution that could lyse 50% of the red blood cells.

Mouse Toxicity Studies. CD1 mice (five per cohort) were intratracheally inoculated with 50 μg/d of native CSP (CSP1 and CSP2) or dnCSPs (CSP1-E1A, CSP2-E1Ad10, CSP1-E1A-cyc(Dap6E10)) for 1 wk. Systemic toxicity was assessed by performing blood chemistry and CBC with differential at the University of Illinois College of Veterinary Medicine Clinical Pathology Laboratory. Histopathology of major organs (lungs, hearts, livers, kidneys, and spleens) and sternum (for genotoxicity) were analyzed at the University of Illinois College of Veterinary Medicine Comparative Pathology Laboratory, as we have previously published (69). Mouse organs were fixed with 10% neutral buffered formalin, embedded in paraffin, sectioned, and stained with haemotoxylin and eosin (H&E). Proinflammatory activities in the lungs were photographed using an Olympus DP70 light microscope.

Downloaded at Palestinian Territory, occupied on December 22, 2021

www.manaraa.com

Mouse Model of Acute Pneumonia. Mouse studies were performed as previously described (60, 61, 68, 74), according to the recommendations in *Guide for the Care and Use of Laboratory Animals* of the NIH (75). The protocol was approved by the Institutional Animal Care and Use Committee at the University of Illinois at Urbana–Champaign (Protocol Number 18135). For the imminent death acute pneumonia studies, 6-wk-old CD1 mice of both sexes (15 to 20 per cohort) (Charles River Laboratories, Inc.) were acclimated for 7 d in positively ventilated microisolator cages with automatic recirculating water, located in a room with laminar, high-efficiency particle accumulation-filtered air. All mice received autoclaved food, water, and bedding. Animals were anesthetized with isoflurane and intranasally administered 5×10^6 CFU pneumococcal cells (in 50 μL). Two hours after infection, mice were intranasally instilled with 100 μg of dnCSPs. Control cohorts received 50 μL of sterile PBS. Mice were monitored every 4 to 12 h for 144 h. Moribund animals that displayed rough hair coat, hunched posture, distended abdomen, lethargy, or inability to eat or drink were considered dead and euthanized. The survival analyses were performed by using the Kaplan–Meier Log Rank (Mantel–Cox) survival test.

Statistical Analysis. Statistical significance of all data was analyzed by using the GraphPad Prism 5.0 package. Data are shown as the mean ± SEM. For two groups, statistical significance was determined by the two-tailed Student's *t* test. To determine the data with three or more groups, two-way ANOVA with Tukey's multiple comparisons test was used. Mouse survival was compared using the Kaplan–Meier Log Rank (Mantel–Cox) survival test. $P < 0.05$ was considered statistically significant.

SI Appendix. Full details of peptide synthesis and characterization, dose response curves for CSP analogs, tables of resonance assignments, and additional structural figures are provided in *SI Appendix*.

ACKNOWLEDGMENTS. This work was supported by NIH Grant R01HL142626 to both Y.T. and G.W.L. Additionally, Y.T. thanks NIH (Grant R35GM128651) for financial support of his laboratory. G.W.L. thanks NIH (Grant R01HL090699) for financial support of his laboratory. This study made use of the National Magnetic Resonance Facility at Madison, which is supported by NIH Grants P41GM103399 and P41GM66326 (National Institute of General Medical Sciences [NIGMS]). Additional equipment was purchased with funds from the University of Wisconsin, NIH (Grants RR02781 and RR08438), NSF (Grants DMB-8415048, OIA-9977486, and BIR-9214394), and the US Department of Agriculture.

1. S. Mehr, N. Wood, *Streptococcus pneumoniae*–A review of carriage, infection, serotype replacement and vaccination. *Paediatr. Respir. Rev.* **13**, 258–264 (2012).
2. J. N. Weiser, The pneumococcus: Why a commensal misbehaves. *J. Mol. Med. (Berl.)* **88**, 97–102 (2010).
3. A. Kadioglu, J. N. Weiser, J. C. Paton, P. W. Andrew, The role of *Streptococcus pneumoniae* virulence factors in host respiratory colonization and disease. *Nat. Rev. Microbiol.* **6**, 288–301 (2008).
4. C. L. F. Walker *et al*., Global burden of childhood pneumonia and diarrhoea. *Lancet* **381**, 1405–1416 (2013).
5. D. Bogaert, R. De Groot, P. W. Hermans, *Streptococcus pneumoniae* colonisation: The key to pneumococcal disease. *Lancet Infect. Dis.* **4**, 144–154 (2004).
6. T. R. Coker *et al*., Diagnosis, microbial epidemiology, and antibiotic treatment of acute otitis media in children: A systematic review. *JAMA* **304**, 2161–2169 (2010).
7. J. P. Lynch , 3rd, G. G. Zhanel, *Streptococcus pneumoniae*: Epidemiology and risk factors, evolution of antimicrobial resistance, and impact of vaccines. *Curr. Opin. Pulm. Med.* **16**, 217–225 (2010).
8. J. Linares, C. Ardanuy, R. Pallares, A. Fenoll, Changes in antimicrobial resistance, serotypes and genotypes in *Streptococcus pneumoniae* over a 30-year period. *Clin. Microbiol. Infect.* **16**, 402–410 (2010).
9. P. K. Mitchell, M. Lipsitch, W. P. Hanage, Carriage burden, multiple colonization and antibiotic pressure promote emergence of resistant vaccine escape pneumococci. *Philos. Trans. R Soc. Lond. B Biol. Sci.* **370**, 20140342 (2015).
10. M. R. Jacobs, Antimicrobial-resistant *Streptococcus pneumoniae*: Trends and management. *Expert Rev. Anti Infect. Ther.* **6**, 619–635 (2008).
11. F. Griffith, The significance of pneumococcal types. *J. Hyg. (Lond.)* **27**, 113–159 (1928).
12. C. Chewapreecha *et al*., Dense genomic sampling identifies highways of pneumococcal recombination. *Nat. Genet.* **46**, 305–309 (2014).
13. N. J. Croucher *et al*., Rapid pneumococcal evolution in response to clinical interventions. *Science* **331**, 430–434 (2011).
14. D. J. Engelmoer, I. Donaldson, D. E. Rozen, Conservative sex and the benefits of transformation in *Streptococcus pneumoniae*. *PLoS Pathog.* **9**, e1003758 (2013).
15. W. P. Hanage, C. Fraser, J. Tang, T. R. Connor, J. Corander, Hyper-recombination, diversity, and antibiotic resistance in pneumococcus. *Science* **324**, 1454–1457 (2009).
16. L. S. Håvarstein, G. Coomaraswamy, D. A. Morrison, An unmodified heptadecapeptide pheromone induces competence for genetic transformation in *Streptococcus pneumoniae*. *Proc. Natl. Acad. Sci. U.S.A.* **92**, 11140–11144 (1995).
17. F. M. Hui, L. Zhou, D. A. Morrison, Competence for genetic transformation in *Streptococcus pneumoniae*: Organization of a regulatory locus with homology to two lactococcin A secretion genes. *Gene* **153**, 25–31 (1995).
18. O. Johnsborg, L. S. Håvarstein, Regulation of natural genetic transformation and acquisition of transforming DNA in *Streptococcus pneumoniae*. *FEMS Microbiol. Rev.* **33**, 627–642 (2009).
19. J. P. Claverys, B. Martin, P. Polard, The genetic transformation machinery: Composition, localization, and mechanism. *FEMS Microbiol. Rev.* **33**, 643–656 (2009).
20. D. A. Morrison, M. S. Lee, Regulation of competence for genetic transformation in *Streptococcus pneumoniae*: A link between quorum sensing and DNA processing genes. *Res. Microbiol.* **151**, 445–451 (2000).
21. G. Pozzi *et al*., Competence for genetic transformation in encapsulated strains of *Streptococcus pneumoniae*: Two allelic variants of the peptide pheromone. *J. Bacteriol.* **178**, 6087–6090 (1996).
22. A. M. Whatmore, V. A. Barcus, C. G. Dowson, Genetic diversity of the streptococcal competence (com) gene locus. *J. Bacteriol.* **181**, 3144–3154 (1999).
23. F. Iannelli, M. R. Oggioni, G. Pozzi, Sensor domain of histidine kinase ComD confers competence pherotype specificity in *Streptoccoccus pneumoniae*. *FEMS Microbiol. Lett.* **252**, 321–326 (2005).
24. O. Johnsborg, P. E. Kristiansen, T. Blomqvist, L. S. Håvarstein, A hydrophobic patch in the competence-stimulating Peptide, a pneumococcal competence pheromone, is essential for specificity and biological activity. *J. Bacteriol.* **188**, 1744–1749 (2006).
25. Y. Yang *et al*., Structure-activity relationships of the competence stimulating peptides (CSPs) in *Streptococcus pneumoniae* reveal motifs critical for intra-group and cross-group ComD receptor activation. *ACS Chem. Biol.* **12**, 1141–1151 (2017).
26. E. V. Pestova, L. S. Håvarstein, D. A. Morrison, Regulation of competence for genetic transformation in *Streptococcus pneumoniae* by an auto-induced peptide pheromone and a two-component regulatory system. *Mol. Microbiol.* **21**, 853–862 (1996).
27. O. Ween, P. Gaustad, L. S. Håvarstein, Identification of DNA binding sites for ComE, a key regulator of natural competence in *Streptococcus pneumoniae*. *Mol. Microbiol.* **33**, 817–827 (1999).
28. M. S. Lee, D. A. Morrison, Identification of a new regulator in *Streptococcus pneumoniae* linking quorum sensing to competence for genetic transformation. *J. Bacteriol.* **181**, 5004–5016 (1999).
29. A. Dagkessamanskaia *et al*., Interconnection of competence, stress and CiaR regulons in *Streptococcus pneumoniae*: Competence triggers stationary phase autolysis of ciaR mutant cells. *Mol. Microbiol.* **51**, 1071–1086 (2004).
30. S. N. Peterson *et al*., Identification of competence pheromone responsive genes in *Streptococcus pneumoniae* by use of DNA microarrays. *Mol. Microbiol.* **51**, 1051–1070 (2004).
31. C. K. Sung, D. A. Morrison, Two distinct functions of ComW in stabilization and activation of the alternative sigma factor ComX in *Streptococcus pneumoniae*. *J. Bacteriol.* **187**, 3052–3061 (2005).
32. G. W. Lau *et al*., A functional genomic analysis of type 3 *Streptococcus pneumoniae* virulence. *Mol. Microbiol.* **40**, 555–571 (2001).
33. M. R. Oggioni *et al*., Switch from planktonic to sessile life: A major event in pneumococcal pathogenesis. *Mol. Microbiol.* **61**, 1196–1210 (2006).
34. J. E. Vidal, K. E. Howery, H. P. Ludewick, P. Nava, K. P. Klugman, Quorum-sensing systems LuxS/autoinducer 2 and Com regulate *Streptococcus pneumoniae* biofilms in a bioreactor with living cultures of human respiratory cells. *Infect. Immun.* **81**, 1341–1353 (2013).
35. S. T. Rutherford, B. L. Bassler, Bacterial quorum sensing: Its role in virulence and possibilities for its control. *Cold Spring Harb. Perspect. Med.* **2**, a012427 (2012).
36. S. B. von Bodman, J. M. Willey, S. P. Diggle, Cell-cell communication in bacteria: United we stand. *J. Bacteriol.* **190**, 4377–4391 (2008).
37. P. Williams, K. Winzer, W. C. Chan, M. Cámara, Look who's talking: Communication and quorum sensing in the bacterial world. *Philos. Trans. R. Soc. Lond. B Biol. Sci.* **362**, 1119–1134 (2007).
38. M. R. Parsek, E. P. Greenberg, Sociomicrobiology: The connections between quorum sensing and biofilms. *Trends Microbiol.* **13**, 27–33 (2005).
39. N. E. Shepherd, R. S. Harrison, D. P. Fairlie, Targeting quorum sensing and competence stimulation for antimicrobial chemotherapy. *Curr. Drug Targets* **13**, 1348–1359 (2012).
40. D. A. Rasko, V. Sperandio, Anti-virulence strategies to combat bacteria-mediated disease. *Nat. Rev. Drug Discov.* **9**, 117–128 (2010).
41. R. W. Mull, A. Harrington, L. A. Sanchez, Y. Tal-Gan, Cyclic peptides that govern signal transduction pathways: From prokaryotes to multi-cellular organisms. *Curr. Top. Med. Chem.* **18**, 625–644 (2018).
42. P. Mayville *et al*., Structure-activity analysis of synthetic autoinducing thiolactone peptides from *Staphylococcus aureus* responsible for virulence. *Proc. Natl. Acad. Sci. U.S.A.* **96**, 1218–1223 (1999).
43. J. S. Wright , 3rd, R. Jin, R. P. Novick, Transient interference with staphylococcal quorum sensing blocks abscess formation. *Proc. Natl. Acad. Sci. U.S.A.* **102**, 1691–1696 (2005).
44. G. J. Lyon, P. Mayville, T. W. Muir, R. P. Novick, Rational design of a global inhibitor of the virulence response in *Staphylococcus aureus*, based in part on localization of the site of inhibition to the receptor-histidine kinase, AgrC. *Proc. Natl. Acad. Sci. U.S.A.* **97**, 13330–13335 (2000).
45. R. J. Scott *et al*., Side-chain-to-tail thiolactone peptide inhibitors of the staphylococcal quorum-sensing system. *Bioorg. Med. Chem. Lett.* **13**, 2449–2453 (2003).
46. Y. Tal-Gan, D. M. Stacy, M. K. Foegen, D. W. Koenig, H. E. Blackwell, Highly potent inhibitors of quorum sensing in *Staphylococcus aureus* revealed through a systematic synthetic study of the group-III autoinducing peptide. *J. Am. Chem. Soc.* **135**, 7869–7882 (2013).

Downloaded at Palestinian Territory, occupied on December 22, 2021

www.manaraa.com

47. Y. Tal-Gan, M. Ivancic, G. Cornilescu, T. Yang, H. E. Blackwell, Highly stable, amide-bridged autoinducing peptide analogues that strongly inhibit the AgrC quorum sensing receptor in *Staphylococcus aureus*. *Angew. Chem. Int. Ed. Engl.* **55**, 8913–8917 (2016).
48. X. Qin, K. V. Singh, G. M. Weinstock, B. E. Murray, Effects of *Enterococcus faecalis* fsr genes on production of gelatinase and a serine protease and virulence. *Infect. Immun.* **68**, 2579–2586 (2000).
49. X. Qin, K. V. Singh, G. M. Weinstock, B. E. Murray, Characterization of fsr, a regulator controlling expression of gelatinase and serine protease in *Enterococcus faecalis* OG1RF. *J. Bacteriol.* **183**, 3372–3382 (2001).
50. K. Nishiguchi, K. Nagata, M. Tanokura, K. Sonomoto, J. Nakayama, Structure-activity relationship of gelatinase biosynthesis-activating pheromone of *Enterococcus faecalis*. *J. Bacteriol.* **191**, 641–650 (2009).
51. D. N. McBrayer, B. K. Gantman, C. D. Cameron, Y. Tal-Gan, An entirely solid phase peptide synthesis-based strategy for synthesis of gelatinase biosynthesis-activating pheromone (GBAP) analogue libraries: Investigating the structure-activity relationships of the *Enterococcus faecalis* quorum sensing signal. *Org. Lett.* **19**, 3295–3298 (2017).
52. D. N. McBrayer, C. D. Cameron, B. K. Gantman, Y. Tal-Gan, Rational design of potent activators and inhibitors of the *Enterococcus faecalis* fsr quorum sensing circuit. *ACS Chem. Biol.* **13**, 2673–2681 (2018).
53. D. N. McBrayer, B. K. Gantman, Y. Tal-Gan, N-methylation of amino acids in gelatinase biosynthesis-activating pheromone identifies key site for stability enhancement with retention of the *Enterococcus faecalis* fsr quorum sensing circuit response. *ACS Infect. Dis.* **5**, 1035–1041 (2019).
54. D. A. Morrison, E. Guédon, P. Renault, Competence for natural genetic transformation in the *Streptococcus bovis* group streptococci *S. infantarius* and *S. macedonicus*. *J. Bacteriol.* **195**, 2612–2620 (2013).
55. G. Salvadori *et al*., Natural transformation of oral Streptococci by use of synthetic pheromones. *Methods Mol. Biol.* **1537**, 219–232 (2017).
56. L. Fontaine *et al*., A novel pheromone quorum-sensing system controls the development of natural competence in *Streptococcus thermophilus* and *Streptococcus salivarius*. *J. Bacteriol.* **192**, 1444–1454 (2010).
57. F. C. Petersen, D. Pecharki, A. A. Scheie, Biofilm mode of growth of *Streptococcus intermedius* favored by a competence-stimulating signaling peptide. *J. Bacteriol.* **186**, 6327–6331 (2004).
58. A. Harrington, Y. Tal-Gan, Identification of *Streptococcus gallolyticus* subsp. gallolyticus (biotype I) competence stimulating peptide pheromone. *J. Bacteriol.* **200**, e00709-17 (2018).
59. C. R. Bikash, S. R. Hamry, Y. Tal-Gan, Structure-activity relationships of the competence stimulating peptide in *Streptococcus mutans* reveal motifs critical for membrane protease SepM recognition and ComD receptor activation. *ACS Infect. Dis.* **4**, 1385–1394 (2018).
60. L. Zhu, G. W. Lau, Inhibition of competence development, horizontal gene transfer and virulence in *Streptococcus pneumoniae* by a modified competence stimulating peptide. *PLoS Pathog.* **7**, e1002241 (2011).
61. B. Koirala, J. Lin, G. W. Lau, Y. Tal-Gan, Development of a dominant negative competence-stimulating peptide (dnCSP) that attenuates *Streptococcus pneumoniae* infectivity in a mouse model of acute pneumonia. *ChemBioChem* **19**, 2380–2386 (2018).
62. Y. Yang, G. Cornilescu, Y. Tal-Gan, Structural characterization of competence-stimulating peptide analogues reveals key features for ComD1 and ComD2 receptor binding in *Streptococcus pneumoniae*. *Biochemistry* **57**, 5359–5369 (2018).
63. Y. Yifang, CSP1-cyc(K6D10). BMRB. https://doi.org/10.13018/BMR30593. Deposited 18 April 2019.
64. Y. Yifang, CSP1-cyc(Orn6D10). BMRB. https://doi.org/10.13018/BMR30594. Deposited 28 March 2019.
65. Y. Yifang, CSP1-cyc(Dab6E10). BMRB. https://doi.org/10.13018/BMR30595. Deposited 18 April 2019.
66. Y. Yifang, CSP1-cyc(Dap6E10). BMRB. https://doi.org/10.13018/BMR30601. Deposited 23 April 2019.
67. Y. Yifang, CSP1-E1A-cyc(Dap6E10). BMRB. https://doi.org/10.13018/BMR30690. Deposited 21 November 2019.
68. L. Zhu, J. Lin, Z. Kuang, J. E. Vidal, G. W. Lau, Deletion analysis of *Streptococcus pneumoniae* late competence genes distinguishes virulence determinants that are dependent or independent of competence induction. *Mol. Microbiol.* **97**, 151–165 (2015).
69. E. I. Parkinson *et al*., Deoxynybomycins inhibit mutant DNA gyrase and rescue mice infected with fluoroquinolone-resistant bacteria. *Nat. Commun.* **6**, 6947 (2015).
70. M. R. Oggioni *et al*., Antibacterial activity of a competence-stimulating peptide in experimental sepsis caused by *Streptococcus pneumoniae*. *Antimicrob. Agents Chemother.* **48**, 4725–4732 (2004).
71. W. Lee, M. Tonelli, J. L. Markley, NMRFAM-SPARKY: Enhanced software for biomolecular NMR spectroscopy. *Bioinformatics* **31**, 1325–1327 (2015).
72. Y. Shen, A. Bax, Protein backbone and sidechain torsion angles predicted from NMR chemical shifts using artificial neural networks. *J. Biomol. NMR* **56**, 227–241 (2013).
73. C. D. Schwieters, J. J. Kuszewski, N. Tjandra, G. M. Clore, The Xplor-NIH NMR molecular structure determination package. *J. Magn. Reson.* **160**, 65–73 (2003).
74. L. Zhu, Z. Kuang, B. A. Wilson, G. W. Lau, Competence-independent activity of pneumococcal EndA [corrected] mediates degradation of extracellular dna and nets and is important for virulence. *PLoS One* **8**, e70363 (2013).
75. National Research Council, Guide for the Care and Use of Laboratory Animals (National Academies Press, Washington, DC, ed. 8, 2011).

Downloaded at Palestinian Territory, occupied on December 22, 2021

www.manaraa.com